scientific reports

Check for updates

OPEN

The cytoglobin-dependent transcriptome in melanoma indicates a protective function associated with oxidative stress, inflammation and cancer-associated pathways

Joey De Backer[1,2] & David Hoogewijs[1]✉

Cytoglobin (CYGB) is a member of the oxygen-binding globin superfamily. In this study we generated stable CYGB overexpressing A375 melanoma cells and performed RNA-sequencing to comprehensively explore the CYGB-dependent transcriptome. Our findings reveal that ectopic expression of CYGB dysregulated multiple cancer-associated genes, including the mTORC1 and AKT/mTOR signaling pathways, which are frequently overactivated in tumors. Moreover, several cancer-associated pathways, such as epithelial-mesenchymal transition (EMT) mediated by *CSPG4*, were downregulated upon CYGB overexpression. Intriguingly, ectopic expression suggested anti-inflammatory potential of CYGB, as exemplified by downregulation of key inflammasome-associated genes, including *NLRP1*, *CASP1* and *CD74*, which play pivotal roles in cytokine regulation and inflammasome activation. Consistent with established globin functions, CYGB appears to be involved in redox homeostasis. Furthermore, our study indicates CYGB's association to DNA repair mechanisms and its regulation of *NOX4*, reinforcing its functional versatility. Additionally, multiple significantly enriched pathways in CYGB overexpressing cells were consistently dysregulated in opposite direction in CYGB depleted cells. Collectively, our RNA-sequencing based investigations illustrate the diverse functions of CYGB in melanoma cells, pointing to its putative roles in cellular protection against oxidative stress, inflammation, and cancer-associated pathways. These findings pave the way for further research into the physiological role of CYGB and its potential as a candidate therapeutic target in melanoma.

Keywords ROS, Oxygen-binding, RNA-seq, Anti-oxidative

Cytoglobin (Cygb) is part of the protein family of mammalian globins in addition to hemoglobin (Hb), myoglobin (Mb), neuroglobin and the more recently identified androglobin[1,2]. The tissue expression pattern of Cygb in mammals has been broadly studied[3]. Cygb is principally expressed in fibroblasts and related cell types, but also in distinct populations of nerve cells. Interestingly, Cygb was found to be highly enriched in melanocytes, and frequently downregulated during melanoma genesis[4]. Although the specific mechanism of action remains to be established, Cygb is hypothesized to function in the cellular response towards oxidative stress[5–9] or is implicated in NO metabolism[10–13].

Substantial research efforts employed animal models to assess the functional role of Cygb in connection to an antioxidant function. Thuy le and colleagues[14] support the antioxidant role of Cygb using a Cygb-deficient mouse model which displays age-dependent development of abnormalities in numerous organs. Liu and co-workers[15] demonstrated Cygb to function as regulator of NO degradation and cardiovascular tone in the vascular wall, consistent with their earlier in vitro findings on the NO dioxygenase function of Cygb[12]. Furthermore,

[1]Section of Medicine, Department of Endocrinology, Metabolism and Cardiovascular System, University of Fribourg, Fribourg, Switzerland. [2]Protein Chemistry, Proteomics and Epigenetic Signaling (PPES) Research Group, Department of Biomedical Sciences, University of Antwerp, Antwerp, Belgium. ✉email: david.hoogewijs@unifr.ch

Cygb-overexpressing transgenic rat models suggested an antifibrotic role of Cygb in renal fibroblasts, possibly via a ROS scavenging mode of action[16,17]. Finally, a recent zebrafish Cygb knockout model displayed phenotypic anomalies and comprehensive transcriptome analysis illustrated altered response to oxidative stress and iron homeostasis as well as modified inflammation related transcripts[18].

Whereas the studies alluded to above mainly focussed on an anti-oxidative role of CYGB, the connection between Cygb and hypoxia in a tumor context has been also extensively investigated[19–23]. Correspondingly, McRonald et al. and Langan et al. have identified Cygb in a background of tylosis with esophageal cancer[24,25]. By employing cell line studies and patient breast and lung cancer material, further evidence was given for a tumor suppressive role of Cygb[26]. Moreover, Shaw and colleagues have shown regulation of Cygb expression by promoter hypermethylation, as well as by tumor hypoxia[27]. Additionally, epigenetic inactivation of Cygb is correlated with poor prognosis in glioma patients[28]. Oleksiewicz et al. described a similar bimodal role for Cygb in lung tumorigenesis, dependent on cell type and microenvironment. Using lung cancer cell lines Cygb is found to function as tumor suppressor under normoxic conditions and as oncogene in cells exposed to hypoxic conditions[29], revealing Cygb as a putative versatile and attractive target for tumor therapy. Furthermore, Cygb overexpression arrests cell cycling at the G1 phase, leading to impaired cell proliferation, potentially by modified phosphorylation of tumour suppressor retinoblastoma protein[30]. Interestingly, S phase kinase-associated protein 2 (Skp2), an oncogenic protein triggering G1/S transition of cell cycle by targeting multiple tumor suppressors and cyclin inhibitors for degradation, has been shown to interact with Cygb and facilitate the periodic degradation of Cygb, to promote cell cycle progression. Additionally, Thuy le et al.[31] and Yassin et al.[32] both reported an implication of Cygb in tumorigenesis using in vivo models. Thuy le et al. described in a murine Cygb-deficient model that the absence of expression of Cygb resulted in an increased incidence of tumor development in the liver and lungs[33]. Subsequently, the group found that Cygb-deficiency leads to an increase in oxidative stress and, in a context of non-alcoholic steatohepatitis, leads to a nearly certain development of hepatocellular carcinoma[31]. Yassin and colleagues reported that Cygb is crucial for the suppression of colorectal tumors[32]. In an independently generated Cygb KO mouse model, Cygb-deficiency exacerbated chemically induced colitis and augmented the establishment of colonic tumors. Cygb-deficient mice were more susceptible to severe inflammation, leading to a significant loss of colonic crypts and colonic epithelial cells[32]. Recently, the Kawada group showed that Cygb attenuates pancreatic cancer growth via scavenging ROS[34]. Several studies have investigated the role of Cygb in cancer in more detail, focusing on its role in hypoxia[35] or as a biomarker for diagnosis and management[36,37]. More recently, analyses on Cygb in the context of tumors suggest that expression of Cygb could be used as a biomarker for early detection of cancer[5], specifically in melanoma.

To expand on these findings, we made use of a melanoma cell model to investigate the potential cellular protective function of CYGB. We generated stable overexpression A375 cells and used RNA sequencing to study the CYGB-dependent transcriptome. Our results are largely consistent with previous in vitro and in vivo models supporting an anti-oxidative role of CYGB and further point to its potential anti-inflammatory function and its divergent association with cancer hallmarks.

Results

RNA sequencing analysis of CYGB overexpressing A375 cells

To explore the consequences of ectopic CYGB expression on the transcriptome of A375 melanoma cells, we performed RNA-seq on A375 control (A375-Ctrl) and CYGB overexpressing A375 cells (A375-hCYGB) under basal conditions. For each genotype, three independent samples were analyzed, and overexpression efficiency was validated on protein and mRNA level by immunoblotting and qPCR, respectively (Fig. 1A and B). Differential analysis of normalized counts using DESeq2 indicated 9595 differentially expressed genes (padj ≤ 0.05), comprising 2778 genes (813 up- and 1956 downregulated) differentially expressed above an absolute log2 fold change of 1 (DEGs; Fig. 2A). Correlation coefficients and principal component analysis (PCA) of the RNA-seq data sets indicated clear separation among A375-Ctrl and A375-hCYGB cells (Supplementary Fig. S3 and S4). Furthermore, box plot visualization of gene expression level distribution reflected reliable sequencing results, since each sample yielded highly similar distribution of the reads (Supplementary Fig. S5). Several of the most pronounced DEGs were validated by qPCR (Fig. 1C).

Subsequently, gene set enrichment analysis (GSEA) was performed to identify enriched sets of genes in the CYGB overexpressing A375 cells relative to the control condition (Fig. 2B; see also Supplementary Fig. S1). fGSEA analysis illustrated that numerous hallmarks were enriched upon CYGB overexpression. The number of genes within each GSEA category are provided in Supplementary Table S1. For example, cell cycle-associated hallmarks G2M checkpoint, E2F targets and mitotic spindle were found to be positively enriched, as well as cancer-related hallmarks MYC targets, MTORC1 (Mammalian target of rapamycin complex 1) signaling, PI3K (phosphoinositide-3-kinase)-AKT-mTOR signaling. Furthermore, hallmarks oxidative phosphorylation, UV response up, reactive oxygen species pathway, DNA repair and unfolded protein response were positively enriched as well. Multiple hallmark pathways were negatively enriched upon CYGB overexpression. Hallmarks TNFα signaling via NF-κB (nuclear factor κ-light-chain-enhancer of activated B cells), Interferon α (IFNα) and IFNγ response, inflammatory response, allograft rejection, and IL6 (interleukin-6)/JAK (janus kinase)/STAT3 (signal transducer and activator of transcription 3) signaling all represent immune-related gene sets. Moreover, cancer-associated hallmarks apical junction, epithelial-mesenchymal transition, myogenesis, estrogen response early, P53 pathway, hypoxia, and KRAS signaling were also negatively enriched in CYGB overexpressing A375 cells.

To further experimentally validate our GSEA analysis and the thereof derived potential immune-protective function of CYGB, we focused on the inflammatory pathway. Consistent with the GSEA analysis we confirmed the CYGB-dependent regulation of caspase-1 (CASP1), cluster of differentiation CD74 and NLR Family Pyrin

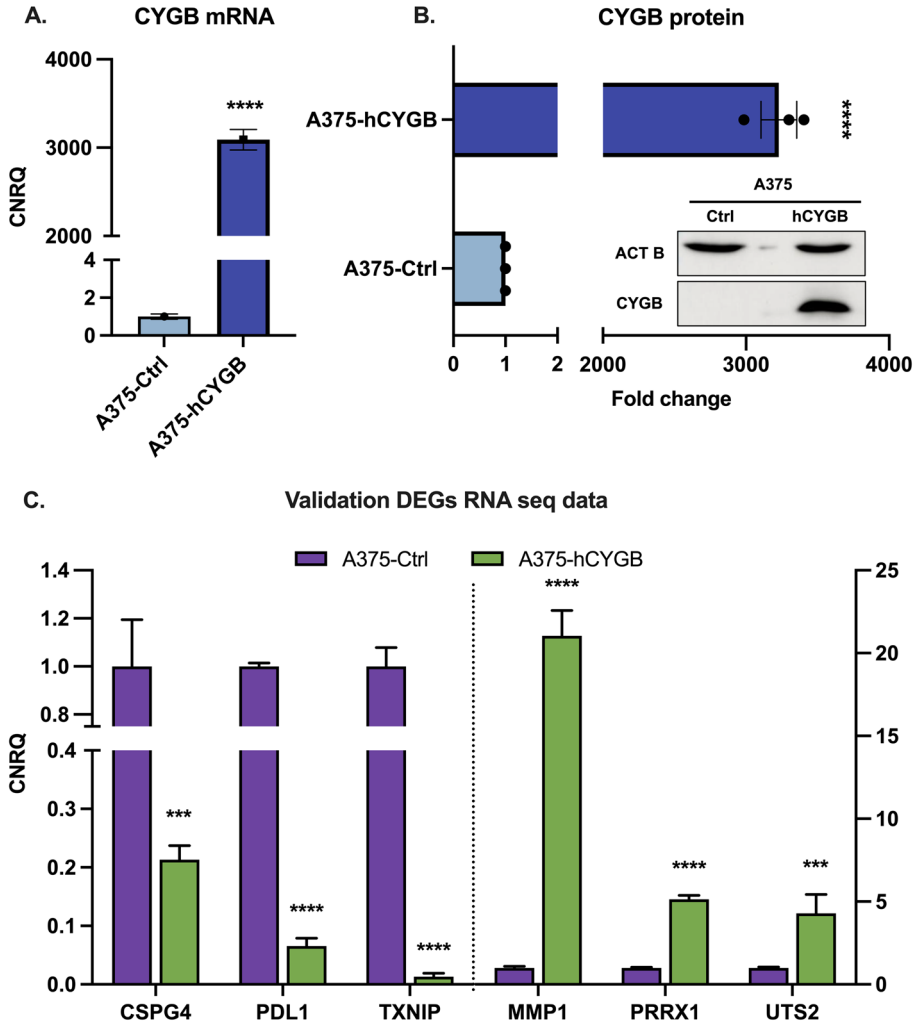

Figure 1. Validation of CYGB overexpression and CYGB-dependent target genes. (**A**) Calibrated normalized relative quantities (CNRQ) of CYGB mRNA in A375 control (A375-Ctrl) and CYGB overexpressing A375-hCYGB cells. CNRQ values measured in A375-Ctrl cells were set at 1. CYGB expression values were normalized to the geometric mean of B2M and YWHAZ expression levels and are represented as mean ± S.E.M values (n = 3). (**B**) Fold change CYGB expression in A375-hCYGB cells compared to A375-Ctrl cells (set at 1). CYGB protein levels were measured with an anti-CYGB antibody, β-actin served as control for equal loading. Original blots are presented in Supplementary Fig. S6. (**C**) Validation of top ranked differentially expressed genes by qPCR. CNRQ values measured in A375-Ctrl were set at 1. Values were normalized to the geometric mean of B2M and YWHAZ expression levels and are represented as mean ± S.E.M values (n = 3). Student-t test (**A**, **B**), Mann–Whitney U test (**C**) (**$p \leq 0.001$; ****$p \leq 0.0001$).

Domain Containing 1 (NLRP1), key inflammasome-associated genes, which are crucial in cytokine regulation and inflammasome activation (Fig. 3).

Following the GSEA-derived redox and immune-related functions of CYGB, the 2778 DEGs were further grouped based on gene ontology (GO) to analyze which biological processes were significantly enriched in CYGB overexpressing A375 cells. The 50 most differentially expressed biological processes together with the associated molecular activities and cellular structures were plotted (Fig. 4). Several of the molecular-level activities performed by gene DEG products are transmembrane transporter activity, ion-(gated) channel activity, Ras guanyl-nucleotide exchange factor activity, receptor regulator activity, and cytokine activity. Some of the larger biological processes, accomplished by multiple molecular activities are extracellular matrix organization, circulatory system process, chemotaxis, reactive oxygen species metabolic process, regulation of inflammatory response, axon development, positive regulation of cytokine production, regulation of signaling receptor activity, and reactive nitrogen species metabolic process. Focusing on the cellular components, most of the DEG products are associated with the extracellular matrix, endoplasmic reticulum lumen, plasma membrane protein complex, collagen trimer, ion channel complex, transmembrane transporter complex, and cell body.

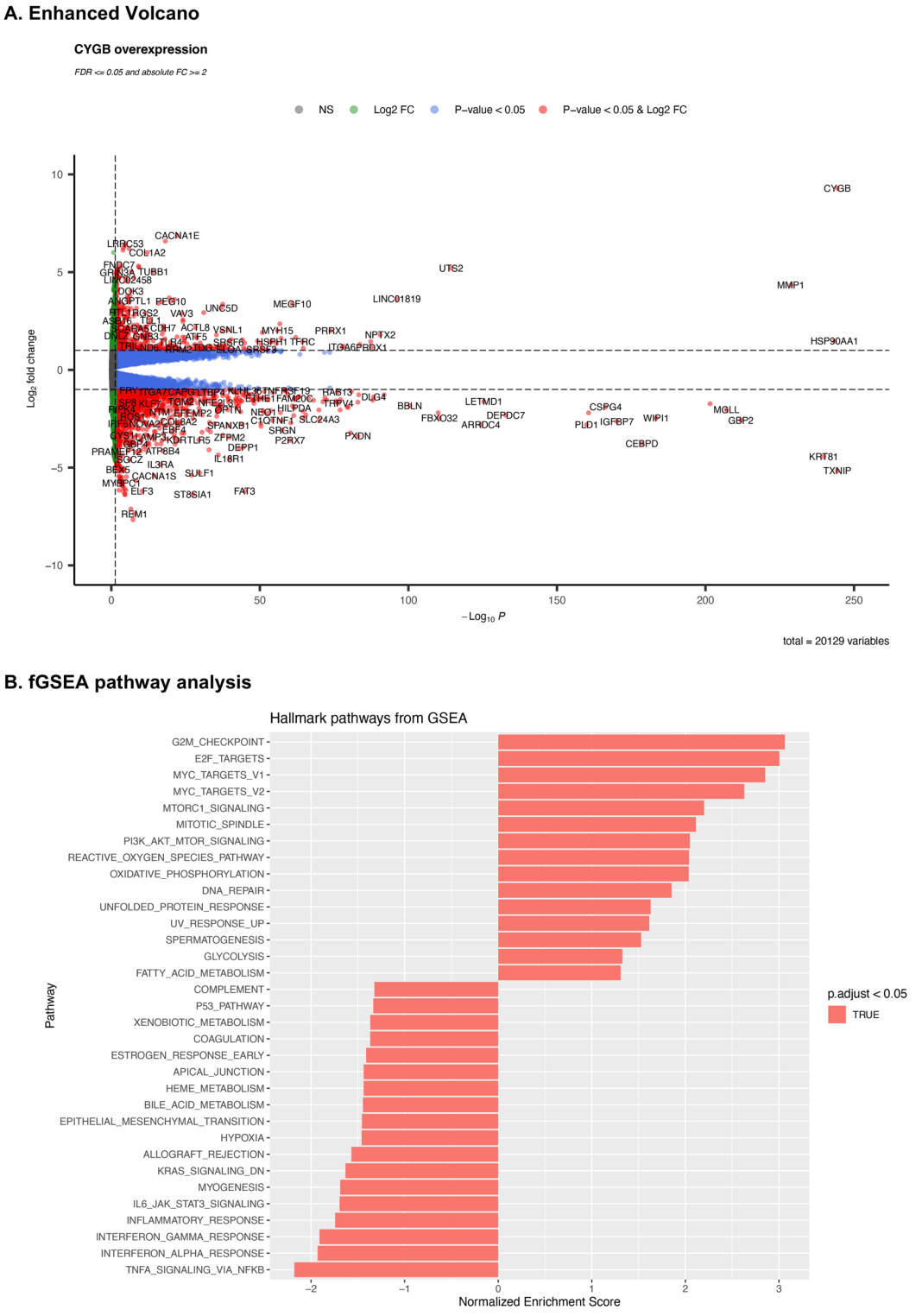

Figure 2. CYGB-dependent transcriptome changes. (**A**) Volcano plot of differentially expressed genes in CYGB overexpressing A375 cells compared to A375-Ctrl cells. The x-axis represents the -Log_{10} p-adjusted value (-Log_{10} P) and the y-axis the Log_2 fold change (Log_2FC). Genes are assigned with specific colors after DESeq2 analysis: gray (not significant [NS]), green (|Log_2FC|> 1), blue (adjusted P < 0.05), or red (|Log_2FC|> 1 and adjusted P < 0.05). (**B**) Fast gene set enrichment analysis (fGSEA) of CYGB overexpressing cells compared to A375-Ctrl cells. Hallmark pathway gene sets were used. Only significantly enriched pathways were shown (p-adjusted value < 0.05).

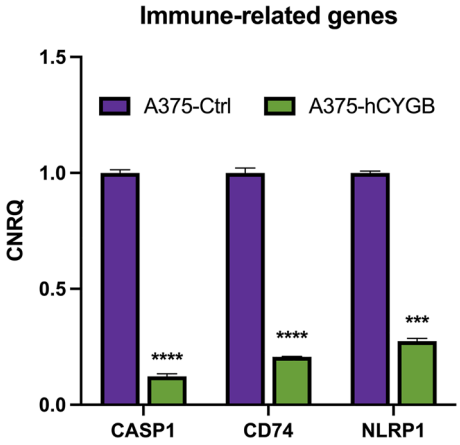

Figure 3. CYGB-dependent regulation of key inflammasome-associated genes. CNRQ values measured in A375-Ctrl cells were set at 1. Values were normalized to the geometric mean of B2M and YWHAZ expression levels and are represented as mean ± S.E.M values (n = 3). Mann–Whitney U test (**$p \leq 0.001$; ****$p \leq 0.0001$).

Comparative gene set enrichment analysis of CYGB depletion versus CYGB overexpression

To investigate a potential more general role of CYGB in redox signaling and immune response in melanoma we integrated data from the melanoma cell line G361 which is endogenously enriched in CYGB and was previously used by us to explore the effect of CYGB knockdown on a transcriptomic level by RNA-seq (GSE209775)[5,9]. In parallel with the current study, differential expression analysis and GSEA was performed between G361 control cells (abundant CYGB expression) and shRNA-mediated CYGB knockdown G361 cells. We therefore extracted the significantly enriched hallmark pathways in the CYGB depleted G361 cells and compared them to the hallmark pathways that were found to be enriched in CYGB overexpressing A375 cells (Fig. 5). Interestingly, many of the positively enriched pathways in CYGB overexpressing A375 cells were negatively enriched in CYGB knockdown G361 cells and vice versa. Whereas CYGB depletion led to upregulation of EMT and apical junction pathways, CYGB overexpression downregulated these pathways. Moreover, oxidative phosphorylation, UV response, immune response, and TNFα signaling via NF-κB were all inversely enriched, positively in CYGB overexpressing A375 cells and negatively enriched in CYGB knockdown G361 cells. It should be noted that 4 out of 12 analyzed pathways were not oppositely enriched, including PI3K-AKT-mTOR signaling, mitotic spindle, E2F targets and G2M checkpoints.

Comprehensive re-analysis of patient-derived primary and metastatic melanoma samples

As the results described above are derived from melanoma cell lines we aimed to strengthen the clinical relevance of our data by further investigating expression data of human primary and metastatic melanoma samples. To this end we performed a comprehensive re-analysis on 2 levels. Firstly, we analyzed expression data comparing 10 isolated melanocytes from frozen human skin samples and 6 primary malignant melanoma samples (dataset GSE238207). Differential expression analysis identified 5591 DEGs of which 2751 were downregulated and 2840 upregulated in primary melanoma samples (Fig. 6B). Several of the top ranked upregulated DEGs including Melan-A (MLANA), Preferentially Expressed Antigen Of Melanoma (PRAME), Premelanosome Protein (PMEL), Tyrosinase (TYR), G Protein-Coupled Receptor 143 (GPR143) and microphthalmia-associated transcription factor (MITF) in primary melanoma are associated with melanomagenesis and pigmentation. However, CYGB expression levels were not significantly dysregulated. Notably, the lincRNA MEG3 (Maternally Expressed 3) was detected among the significantly downregulated genes, similar to our previously obtained cell line-based data with depleted CYGB levels. To evaluate pathway enrichment in the transcriptional data we performed fGSEA analysis (Fig. 6A). The number of genes within each GSEA category are provided in Supplementary Table S2. Seventeen pathways were positively enriched in primary malignant melanoma samples of which some were linked to metabolism, cell cycle and proliferation, and oxidative stress. Interestingly, most of the 18 hallmark pathways that were negatively enriched in primary melanoma samples were associated with the immune response (complement, interferon γ response, TNFα via NFκB, IL2/STAT5 signaling, IL6/JAK/STAT3 signaling, inflammatory response, allograft rejection, estrogen response early, TGFβ signaling). The remaining hallmark pathways KRAS signaling (up), epithelial-mesenchymal-transition (EMT), apical junction, myogenesis, angiogenesis, apoptosis, and coagulation are typically associated with cancer development, progression, and invasiveness.

Apart from primary malignant melanoma, we also included expression data from 82 patient-derived metastatic melanoma samples (GSE29359) compared to 7 human primary melanocyte cell lines. Differential expression analysis identified 1370 differentially expressed genes of which 738 were downregulated and 612 upregulated in metastatic melanoma samples compared to primary melanocytes (Fig. 7B). Similar as for the primary malignant melanoma data we performed fGSEA analysis to evaluate pathway enrichment (Fig. 7C). The number of genes within each GSEA category are provided in Supplementary Table S3. Fifteen pathways were

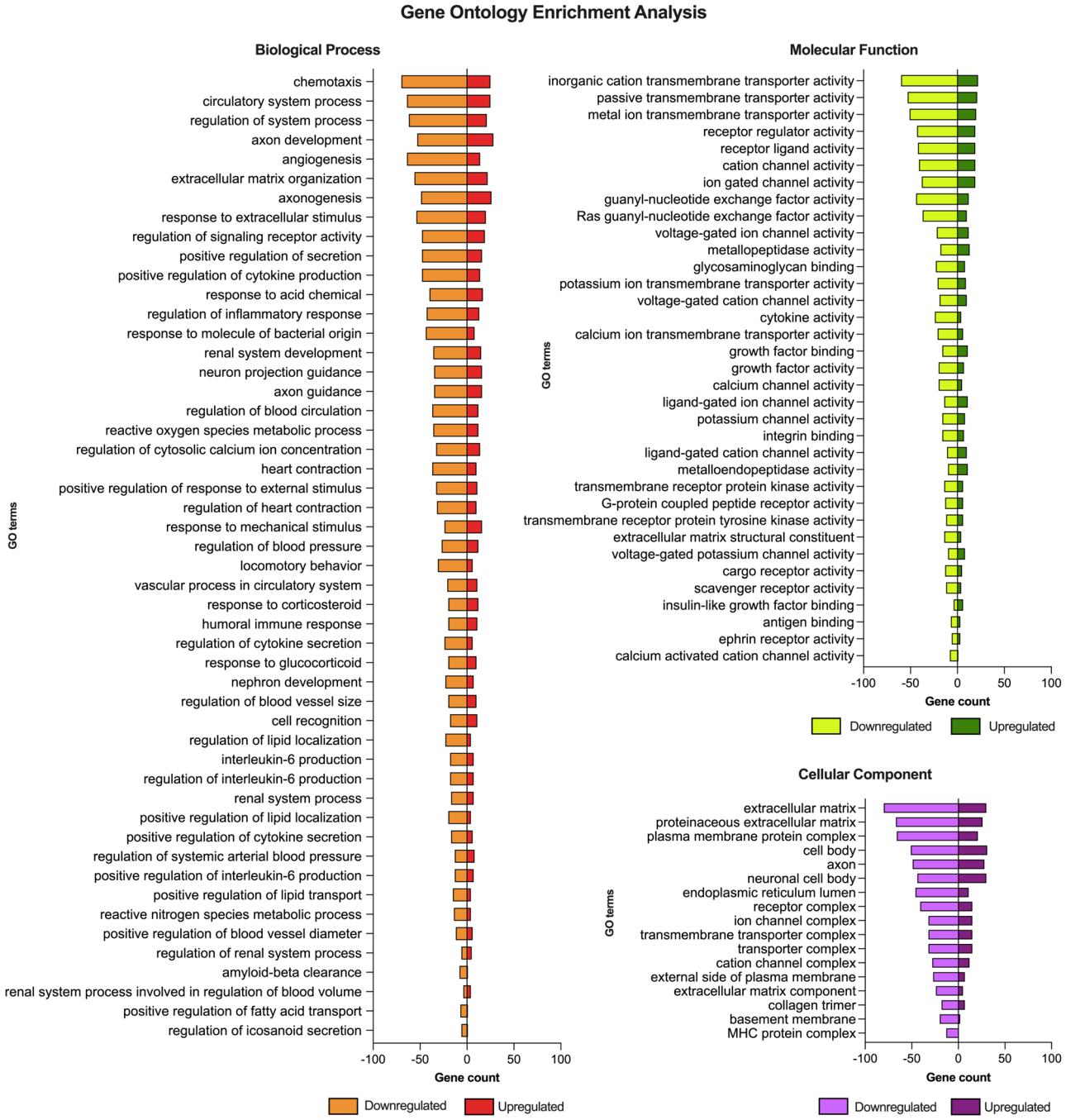

Figure 4. Gene ontology analysis. Top enriched gene ontology (GO) terms associated with the differentially expressed genes (DEGs) in CYGB overexpressing A375 cells. The number of DEGs that contributed to the enrichment of a specific GO term through its down- or upregulation is shown for each GO term. GO terms were ranked according from highest counts to lowest counts. Molecular function terms describe molecular-level activities executed by gene products. Biological process terms refer to larger processes accomplished by several molecular activities. The cellular component terms illustrate the functional locations relative to cellular structures of the gene products.

positively enriched in metastatic melanoma of which more than half were immune-related (allograft rejection, interferon γ and α response, IL2/STAT5 signaling, IL6/JAK/STAT3 signaling, inflammatory response, TNFα via NFκB, complement, and estrogen response late). The remaining hallmark pathways KRAS signaling (up), EMT, apical junction, myogenesis, hypoxia, and coagulation are typically associated with cancer development, progression, and invasiveness. In contrast, metabolism-associated pathways oxidative phosphorylation, fatty acid transport, adipogenesis, heme-metabolism were negatively enriched in metastatic melanoma samples. Androgen response, MYC targets, and protein secretion were also found to be negatively enriched. Among

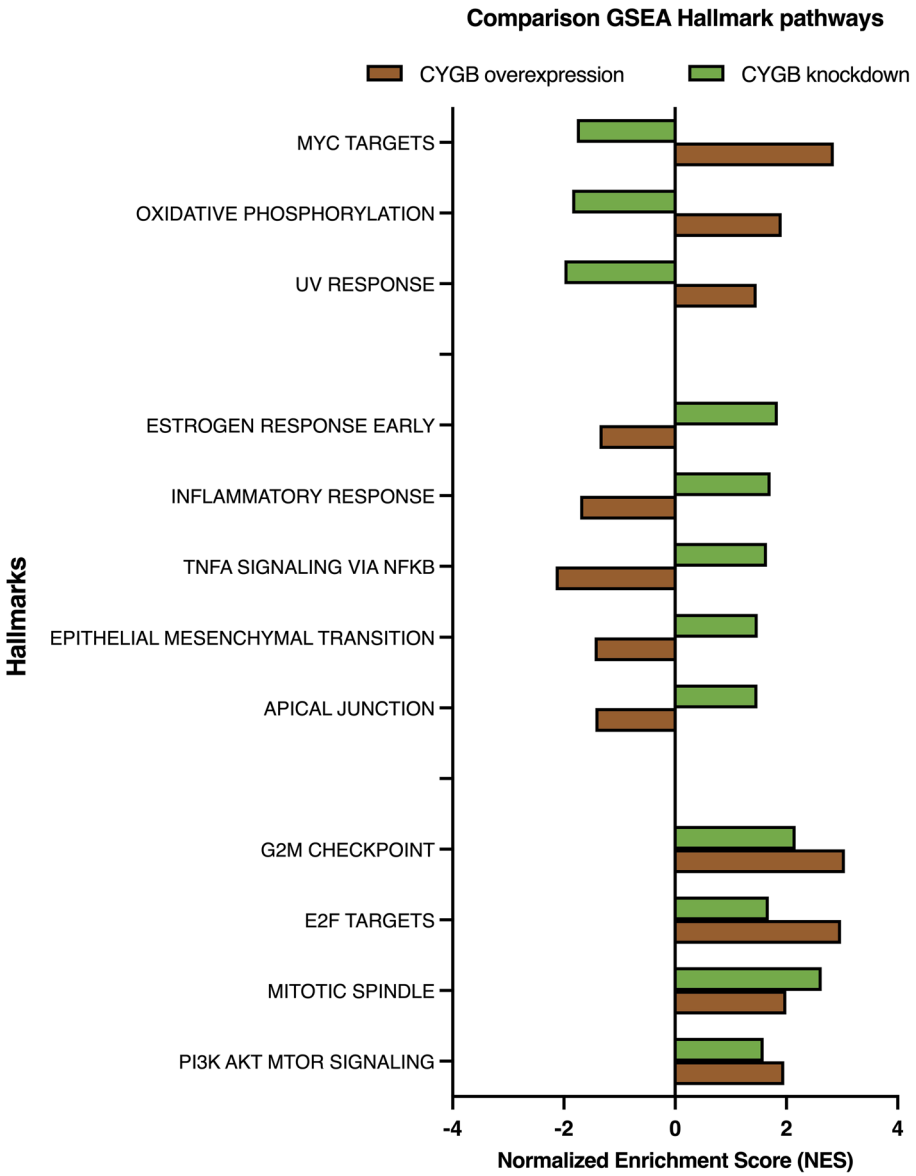

Figure 5. Comparative GSEA analysis of hallmark pathways. Significantly enriched hallmark pathways in CYGB overexpressing A375 cells were compared to the hallmark pathways that were enriched in CYGB knockdown G361 cells (data available from: GSE209775) based on Normalized Expression Scores (NES). Hallmark pathways were ordered first accordingly to being enriched after CYGB overexpression, then after CYGB downregulation, and subsequently without opposite effect. In each of the groups, hallmark pathways were ordered from the highest to the lowest NES scores.

the top ranked differentially expressed genes were the microphthalmia-associated transcription factor (MITF) and cluster of differentiation CD74. More importantly, CYGB was one of the DEGs found downregulated in metastatic melanoma samples (Fig. 7A and B). However, CYGB expression was highly variable amongst the individual melanoma samples, with some samples expressing CYGB to the same extent as primary melanocytes. We therefore divided the metastatic melanoma samples in a 'CYGB-low' and a 'CYGB-high' expressing group and subsequently performed a differential expression analysis followed by an enrichment analysis using the biological process gene ontology aspect (Fig. 8). 1162 DEGs were identified of which 617 were upregulated and 548 downregulated (Fig. 8A). When considering the top biological processes, several terms related to cell division (i.e., mitotic cell cycle, chromosome organization) were activated in CYGB-low melanoma cells (Fig. 8B). In contrast, extracellular matrix organization and cell adhesion were suppressed in CYGB-low cells compared to CYGB-high cells, possibly indicating that metastatic melanoma cells with low CYGB expression levels have a more aggressive cancer phenotype compared to melanoma cells displaying high CYGB expression levels.

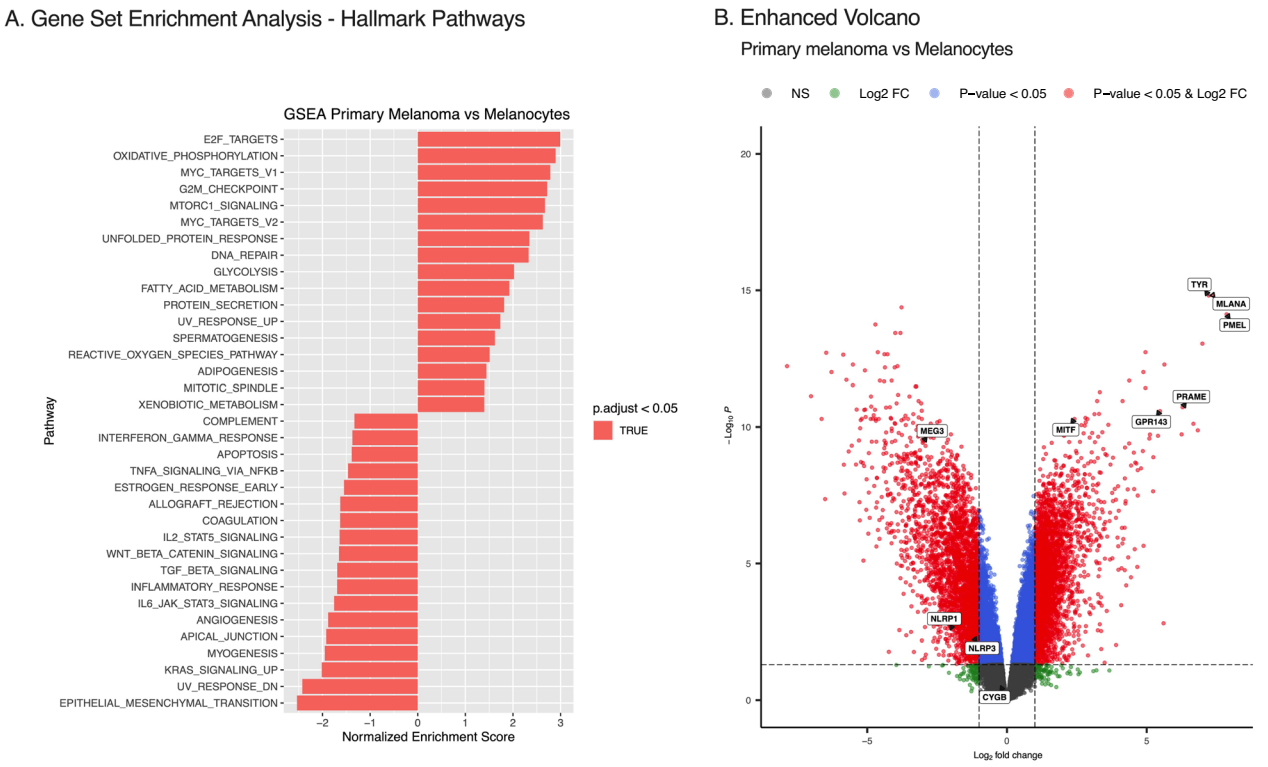

Figure 6. Comprehensive re-analysis of human primary malignant melanoma samples. (**A**) Fast gene set enrichment analysis (fGSEA) of primary malignant melanoma samples compared to isolated melanocytes. Hallmark pathway gene sets were used. Only significantly enriched pathways were shown (p-adjusted value < 0.05). (**B**) Volcano representation of the differential expression analysis of primary malignant melanoma samples. The genes CYGB, NLRP1, NLRP3, MITF, MEG3, GPR143, PRAME, PMEL, MLANA, and TYR have been labeled in boxes. Differentially expressed genes were represented based on their Log_2 fold change (Log_2FC) and $-Log_{10}$ p-adjusted value ($-Log_{10}$ P). Genes are assigned with specific colors after DESeq2 analysis: gray (not significant [NS]), green ($|Log_2FC| > 1$), blue (adjusted $p < 0.05$), or red ($|Log_2FC| > 1$ and adjusted $p < 0.05$).

Discussion

Transcriptomic analysis of CYGB overexpressing A375 cells, a cell line with low endogenous CYGB levels, showed that CYGB is involved in numerous pathways and cellular activities. Ectopic CYGB expression led to the positive enrichment of several cancer-associated pathways. Mammalian target of rapamycin complex 1 (mTORC1) mainly regulates cell growth and metabolism[38]. mTOR is implicated in multiple signaling pathways throughout the body, including phosphoinositide-3-kinase (PI3K)/AKT and several studies have shown that tumors typically over-activate the AKT/mTOR signaling pathway[39,40]. Moreover, AKT controls the stability of the proto-oncogene MYC through mTORC1[41]. MYC generally acts as a transcription factor coordinating multiple biological processes and is able to induce tumorigenesis by evading multiple tumor-suppressing checkpoint mechanisms, including proliferative arrest, apoptosis, and/or senescence[42]. However, other cancer-associated pathways were rather negatively enriched. Oncogenic KRAS promotes cell survival, proliferation, and cytokine secretion, including cytokine TNFα, which in turn activates nuclear factor κ-light-chain-enhancer of activated B cells (NF-κB), which promotes tumor metastasis and invasiveness[43,44]. Epithelial—mesenchymal transition (EMT) transforms polarized epithelial cells into motile mesenchymal cells, thereby facilitating invasiveness and metastasis[45]. Furthermore, the top biological process identified among the DEGs clearly indicated downregulation of genes involved in the organization of the extracellular matrix (Fig. 4). Moreover, chondroitin sulfate proteoglycan 4 (*CSPG4*) was found to be downregulated upon CYGB overexpression (Fig. 1C). CSPG4 activation of the focal adhesion kinase (FAK) pathway and/or mitogen-activated protein kinase/extracellular signal-regulated kinase (MAPK/ERK) pathway[46], enables the regulation of several cellular functions driving reorganization of the cytoskeleton, survival and chemoresistance, invasion, migration and proliferation, as well as EMT transition in the radial growth phase of human melanomas[47–49].

Interestingly, the hallmark oxidative phosphorylation was positively enriched whereas hallmark hypoxia was negatively enriched. Therefore, it seems that CYGB overexpression led to higher oxygenation levels and thus subsequent downregulation of genes that are involved in the response to hypoxia. Increased oxygenation levels could then possibly lead to increased oxidative phosphorylation. This is aligning well with a previous study performed in our group, where we found that knockdown of CYGB in G361 melanoma cells, with abundant endogenous CYGB expression levels, diminished mitochondrial oxidative phosphorylation[5]. Furthermore, many of the hallmarks that were either positively or negatively enriched in CYGB overexpressing A375 cells were

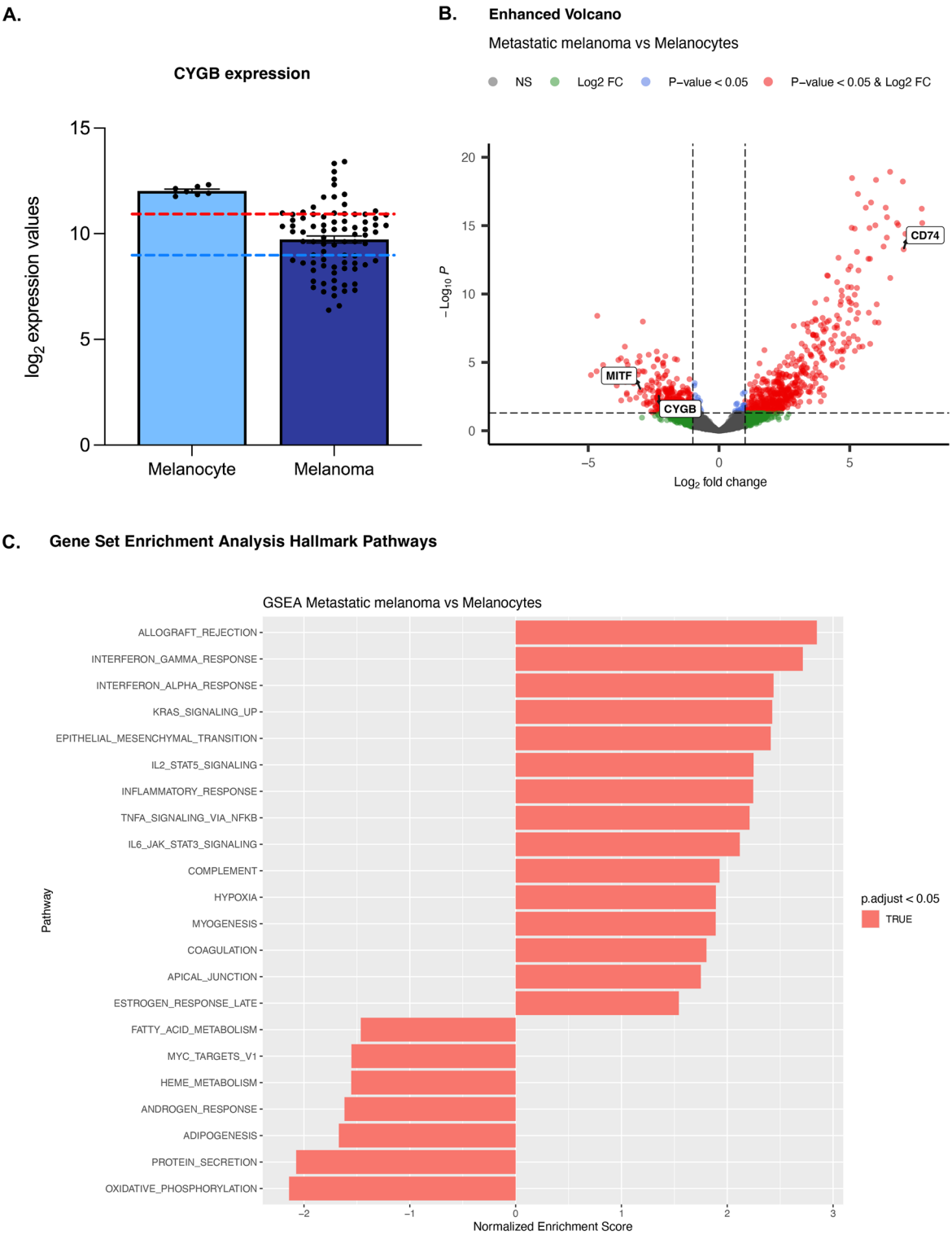

Figure 7. Comprehensive re-analysis of human metastatic melanoma samples. (**A**) Differential gene expression analysis of CYGB using the whole genome bead array dataset (GSE29359) comparing 7 human primary melanocyte cell lines and 82 patient-derived metastatic melanoma samples. CYGB is differentially expressed in melanoma cells. Expression is represented as Log2 (normalized) expression values. Blue line: upper limit CYGB-low melanoma samples; red line: lower limit CYGB-high melanoma samples. (**B**) Volcano representation of the differential expression analysis of melanoma samples. The genes CYGB, MITF and CD74 have been labeled in boxes. Differentially expressed genes were represented based on their Log_2 fold change (Log_2FC) and $-Log_{10}$ p-adjusted value ($-Log_{10}$ P). Genes are assigned with specific colors after DESeq2 analysis: gray (not significant [NS]), green ($|Log_2FC| > 1$), blue (adjusted $P < 0.05$), or red ($|Log_2FC| > 1$ and adjusted $p < 0.05$). (**C**) Fast Gene Set Enrichment Analysis (fGSEA) of metastatic melanoma samples compared to primary melanocytes. Hallmark pathway gene sets were used. Only significantly enriched pathways were shown (p-adjusted value < 0.05).

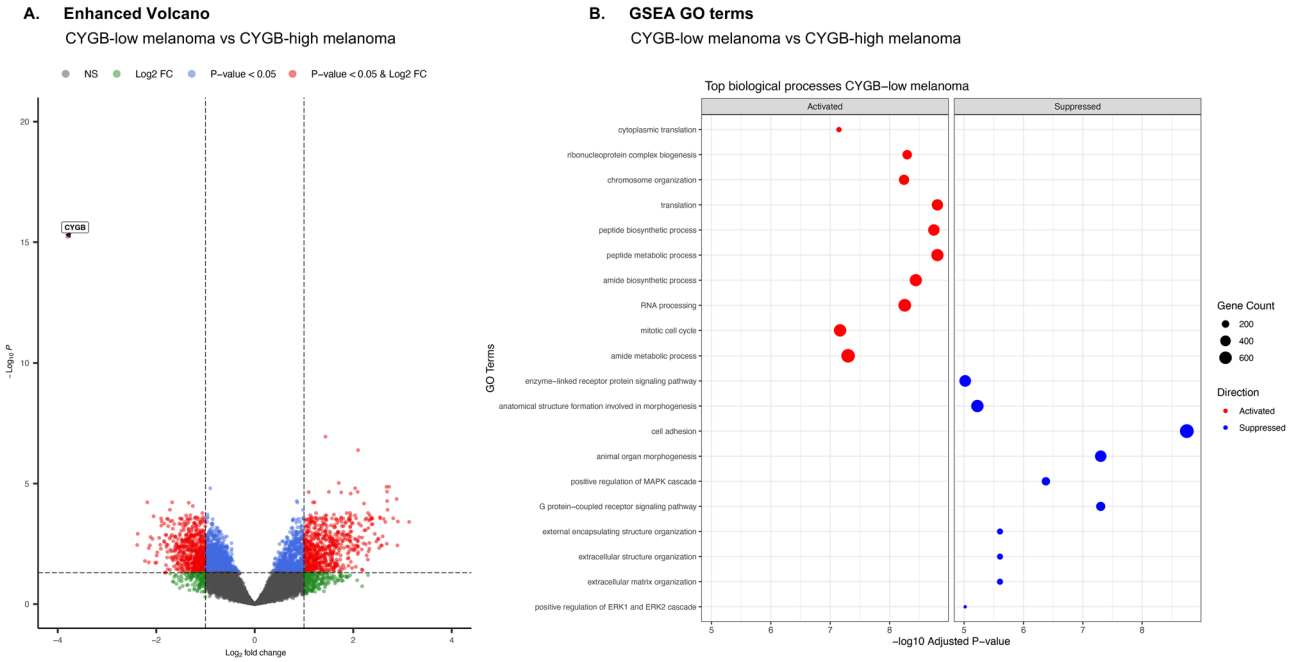

Figure 8. (**A**) Volcano representation of the differential expression analysis of CYGB-low versus CYGB-high metastatic melanoma. CYGB has been labeled. Differentially expressed genes were represented based on their Log_2 fold change (Log_2FC) and $-Log_{10}$ p-adjusted value ($-Log_{10}$ P). Genes are assigned with specific colors after DESeq2 analysis: gray (not significant [NS]), green ($|Log_2FC| > 1$), blue (adjusted $P < 0.05$), or red ($|Log_2FC| > 1$ and adjusted $p < 0.05$). (**B**) Fast Gene Set Enrichment Analysis (fGSEA) of CYGB-low versus CYGB-high metastatic melanoma samples using the biological processes Gene Ontology (GO) aspect. The top 20 activated and suppressed GO terms in CYGB-low metastatic melanoma cells are shown. Gene ratio represents the number of differentially expressed genes against the number of genes associated with a GO term.

inversely enriched in CYGB-depleted G361 melanoma cells (Fig. 5), confirming the involvement of CYGB in these pathways. Only 4 out of 12 analyzed pathways were not oppositely enriched, possible due to biological variation. The general consistency in CYGB-dependent transcriptome between ectopic CYGB expression in a melanoma cell line with low endogenous CYGB expression levels and shRNA-mediated knockdown of CYGB in a cell line with abundant endogenous CYGB expression levels further underscores the validity of our transcriptomic findings and may hint to a broader role of CYGB in melanoma as well as its potential as a therapeutic target.

Remarkably, most of the negatively enriched hallmarks in CYGB overexpressing cells are immune-related (Fig. 2B). This was further highlighted in the GO analysis of the DEGs where genes related to the regulation of the inflammatory response were mostly downregulated (Fig. 3). Additionally, genes responsible for cytokine production in general, and interleukin-6 (IL-6) production specifically, were overall downregulated. Moreover, we previously showed that treatment with the ferroptosis inducer (1S, 3R)-RAS-selective lethal small molecule (RSL3) in CYGB-depleted G361 cells led to the activation of the NOD-, LRR- and pyrin domain-containing protein 3 (NLRP3) inflammasome and subsequent induction of pyroptosis[5]. In the current study, upon close evaluation of the DEGs of immune-associated hallmarks and biological processes we found that the genes involved in inflammasome activation were downregulated in CYGB overexpressing cells. For example, *NLRP1* and caspase 1 (*CASP1*) were significantly downregulated, as well as cluster of differentiation *CD74* (Fig. 2A and Supplementary Fig. S2). These genes were experimentally validated by qPCR experiments on independent samples (Fig. 3). NLRP1 and CASP1 transcription is initiated by regulation of the activation of pathogen-associated molecular patterns, toll-like receptors (TLRs) or cytokines such as TNFα and IL-1β promoting NF-κB activation and subsequent gene transcription[58]. Consistently, our observations in the current study illustrate enrichment of hallmark pathway TNFα via NF-κB signaling and downregulation of the potent pyrogen gene *IL1B*.

Taken together, transcriptome analysis of ectopic CYGB expression in A375 melanoma cells suggests that CYGB seems to reduce the inflammatory state of these cells. Numerous studies indicated an anti-inflammatory function for CYGB via regulation of the cytokines TNFα and IL-6 through inhibition of the NF-κB pathway, consistent with the RNA-seq data in the current study[18,32,50]. Additionally, lipopolysaccharide-induced nicotinamide adenine dinucleotide phosphate (NADPH) oxidase activity and ROS generation was shown to be inhibited by CYGB[51]. Considering that ROS and RNS are important drivers of inflammation, CYGB could possibly regulate and/or attenuate inflammation through its intrinsic and polyvalent RONS-scavenging functions. CYGB's involvement in the regulation of redox homeostasis is evidenced further in the fGSEA and GO analysis presented here, as hallmark reactive oxygen species pathway and reactive oxygen/nitrogen species metabolic processes were enriched in CYGB overexpressing A375 cells (Figs. 2B and 4). Peroxiredoxin-1 (*PRDX1*) and glutathione peroxidase 3 (*GPX3*) were among the few DEGs that were upregulated, whereas also

glutamate-cysteine ligase regulatory subunit (*GCLM*), a gene encoding a key enzyme of glutathione synthesis was upregulated (Supplementary Fig. S2). On the other hand, NADPH Oxidase Activator 1 (*NOXA1*), Dual Oxidase Maturation Factor 1 (*DUOXA1*) and NADPH Oxidase 4 (*NOX4*), genes directly involved in ROS production, were downregulated. Thus, it seems that the presence of CYGB fortifies the defense against oxidative stress by upregulating ROS-scavenging genes and downregulating ROS-producing genes. Noteworthy, the superoxide dismutase 2 gene *SOD2* was one of the downregulated DEGs. Although a previous investigation[52] suggested absence of SOD function, a more recent study[53] demonstrated a potent SOD activity for CYGB and indicated that in smooth muscle cells exposed to oxidative stress CYGB plays a crucial function in the metabolism of superoxide and protects the cells against superoxide-mediated death. Indeed, it is conceivable that due to ectopic CYGB expression, the cell's need for other SOD enzymes is reduced.

Another intriguing finding derived from our transcriptome results is a link to a very recent study suggesting a role of CYGB in NOX4-dependent inhibition of DNA damage. Mathai and colleagues[54] provide an elegant mechanism by which NOX4 and H_2O_2 first promote nuclear translocation of CYGB to enable CYGB to regulate transcriptional output and inhibit DNA damage through interaction with HMGB2, a non-histone chromatin structural protein. Our results would corroborate with this study as the hallmark DNA repair is enriched and NOX4 is CYGB-dependently regulated (Supplementary Fig. S2). Although the hallmark DNA repair is rather positively enriched, context-dependent, or condition-dependent effects cannot be excluded.

To complement and strengthen our cell line-based data with clinical samples we explored two distinct transcriptome datasets comprising 6 primary malignant and 82 metastatic patient-derived melanoma samples, displaying multiple differentially expressed genes. For instance, the melanocyte-specific transcription factor MITF was significantly downregulated in metastatic melanoma samples (Fig. 7B). MITF is essential for the differentiation, proliferation and survival of melanocytes but is also known as a driver of melanoma progression[55]. MITF expression and activity is highly variable between different melanoma tumors[56]. However, melanoma with low MITF expression has been shown to be more invasive (metastatic). Remarkably, MITF was upregulated in primary melanoma samples. CD74 was also one of the most pronounced upregulated DEGs in metastatic melanoma. This is in accordance with previous studies illustrating abundant CD74 expression in both melanoma cell lines (including A375) and tissues[57–59]. Moreover, Tanese et al. found that IFN-γ enhances the expression of CD74 which subsequently, through interaction with its ligand macrophage migration inhibitory factor (MIF), activates the PI3K/AKT pathway and promotes tumor survival. Although the pathway PI3K/AKT via mTOR signaling was positively enriched in CYGB overexpressing A375 cells, IFN-γ response was negatively enriched and, more importantly, CD74 was accordingly identified as a DEG downregulated in A375-hCYGB (Figs. 2B and 3). Additionally, blockade of CD74-MIF interaction reduced the expression of pro-tumorigenic molecules, including IL-6[58]. The reduced production of IL-6 observed in our transcriptome study (Fig. 4) would be clearly consistent with this decreased expression of pro-tumorigenic molecules. However, the use of A375 as single melanoma cell line might represent a potential limitation and future investigations should explore the consistency of CYGB-dependently regulated effects in additional cell lines.

Melanoma is one of the most immunogenic tumors[60,61], which is also evident from the GSEA re-analysis of metastatic melanoma illustrating multiple immune-related pathways (Fig. 7). Overexpression of CYGB in A375 cells led to the downregulation of these pathways. Accordingly, CYGB knockdown in G361 melanoma cells upregulated several immune pathways (Fig. 5). Considering that some melanoma cells retain high levels of CYGB expression, CYGB could influence the outcome of immune therapy. Therefore, CYGB could have potential use as a marker for treatment outcome. It is striking however that most of the significantly downregulated hallmark pathways in primary malignant melanoma were immune-related. The expression levels of NLRP1 and NLRP3 were also downregulated, further suggesting an ameliorated inflammatory state (Fig. 6B). Thus, it seems that during the progression of melanoma from primary (with unchanged CYGB expression levels) to metastatic melanoma (with low CYGB expression), the immune response is altered, indicating a shift towards a more inflammatory state during this transition, possibly influenced by CYGB expression. It would be interesting to further investigate CYGB expression in a larger cohort and/or experimentally modulate CYGB expression levels to explore its effect on the immune signature.

In conclusion, by analyzing the CYGB-dependent transcriptome in an ectopic context this study explores the broad functions of CYGB in melanoma cells, illustrating its possible roles in cellular protection against oxidative stress, inflammation, and cancer-associated pathways. Our data open novel avenues to further elucidate the underlying molecular mechanism of CYGB's protective role and hint to its potential as a target for therapeutic interventions in melanoma as well as to its potential as a marker for treatment outcome. Follow-up studies in additional cell lines remain to be conducted to further validate the applicability of our study.

Methods

Cell culture

A375 melanoma cells (CRL-1619IG-2) were procured from ATCC (Manassas, VA, USA) and cultured in Dulbecco's Minimum Essential Media (DMEM) (Gibco, Life Technologies; Waltham, MA, USA). The DMEM was enriched with L-glutamine and supplemented with 10% heat-inactivated fetal bovine serum (FBS) sourced from Gibco, (Fisher Scientific, Waltham, MA, USA) as well as 1% Penicillin/Streptomycin (10,000 Units/mL P; 10,000 µg/mL S; Gibco, Life Technologies). These cells were maintained at 37 °C in a controlled environment with humidified atmosphere containing 5% CO_2 and were regularly subcultured following trypsinization.

Establishment of a stable CYGB overexpression cell model

To produce stably transfected A375 cell lines the human *CYGB* gene and the control gene β-glucuronidase (*GUS*) were first inserted into a pLENTI6 plasmid (Invitrogen). Viral particles were generated in HEK293T cells by

co-transfection of the respective transfer vector (3 µg) with the packaging plasmids pLP1 (4.2 µg), pLP2 (2 µg) and pVSV-G (2.8 µg, all from Invitrogen) using the $CaCl_2$ transfection method as reported earlier[62]. A375 cells were subsequently transduced with lentiviral-pseudotyped particles and pools of A375-hCYGB cells and A375-GUS cells (referred to as A375-Ctrl cells) were further cultured in the indicated medium supplemented with blasticidin.

RNA extraction, purification and cDNA conversion

For RNA extraction and purification, we utilized the PureLink RNA Kit (Invitrogen, Waltham, MA, USA), following the protocol provided by the manufacturer. Subsequently, we assessed RNA concentration and purity by analyzing the absorbance at a 260/280 nm ratio using an Epoch spectrophotometer (BioTek, Winooski, VM, USA). To generate cDNA we employed 1 µg of RNA and performed reverse transcription with Superscript II reverse transcriptase from Invitrogen, as described before[63,74].

Quantitative PCR

We employed the StepOne Real-Time PCR system (Applied Biosystems, Waltham, MA, USA) using a Power SYBR Green Master Mix (Applied Biosystems) for measuring mRNA levels. For the three biological replicates duplicate PCR reactions were performed. qbase + software (version 3.2; https://cellcarta.com/genomic-data-analysis/; Biogazelle, Zwijnaarde, Ghent, Belgium) was employed to analyze expression data, as described before[64]. Supplementary Table S4 provides details of oligonucleotide sequences for amplification of CYGB, TXNIP, PLD1, CSPG4, USP2, MMP1, PRRX1, NLRP1, CD74, CASP1, B2M and YWHAZ. Oligonucleotides were manufactured by Eurogentec (Seraing, Liège, Belgium).

Protein extraction and quantification

To lyse the cells, we utilized a lysis buffer, consisting of 10 mM Tris HCl (pH 8), 1 mM EDTA, 400 mM NaCl, 1% NP-40 and protease inhibitors (Sigma-Aldrich, Burlington, MA, USA), following a previously described protocol[65]. The lysed cells were gently agitated on a rotating platform at 4 °C for 30 min to ensure optimal action of the lysis buffer. Subsequently, the suspension underwent sonication for 1 min at 60 Hz to disperse any potential DNA aggregates. Afterwards, samples were subjected to centrifugation at 10,000 × g for 15 min to collect the protein-containing supernatant. Finally, the BCA method was applied to quantify protein concentrations with a kit (ThermoFisher Scientific, Waltham, MA, USA).

Immunoblotting

For immunoblotting of extracted proteins, we initially separated them according to molecular weight using sodium dodecyl sulphate polyacrylamide gel electrophoresis (SDS-PAGE) gels, followed by electrotransfer onto nitrocellulose membranes (Amersham Hybond-ECL, GE Healthcare, Chicago, IL, USA), as previously described[66,67]. For CYGB immunoblotting we employed 12.5% polyacrylamide gels. Subsequently, membranes were blocked in TBS-T (Tris-buffered saline; 0.1% Tween-20), containing 5% non-fat dry milk, for 1 h at room temperature. Overnight incubation of membranes was done at 4 °C with primary antibodies (anti-CYGB, 1:500 dilution, Proteintech, Rosemont, IL, USA; 13,317–1-AP; anti-β-Actin (ACTB) 1:5000 dilution, Santa Cruz, sc-47778). The subsequent day, membranes were washed with TBST-T and incubated for 1 h with horseradish-conjugated secondary antibodies (anti-rabbit IgG HRP 1:5000 dilution, Sigma, GENA934-1ML; anti-mouse IgG HRP, 1:10,000 dilution, Invitrogen, 31,430). Signals were visualized with ECL Prime (Amersham, GERPN2232) on an Amersham Imager 680 (GE Life Sciences; Piscataway, NJ, USA) and subsequently exported and quantified with Image Studio™ software (version 5.2.5; https://www.licor.com/bio/image-studio/; LI-COR Biosciences, Lincoln, NE, USA).

RNA sequencing

The initial step involved evaluation of total RNA sample quality, which was accomplished through assessment using the TapeStation (Agilent Technologies, Santa Clara, CA, USA) and the Qubit assay (Invitrogen). For subsequent experiments we selected total RNA samples with an RNA integrity number (RIN) > 7.0 and purity (OD260/OD280) ratio 1.8–2.2. To conduct sequence libraries, we employed the poly(A) RNA selection approach, creating a distinct library for each of the triplicate samples. High-throughput RNA sequencing was conducted, employing pair-end 150 bp reading length on an Illumina NovaSeq 6000 (Illumina, San Diego, CA, USA) sequencer. We employed DESeq2 (version 1.40.2) analysis in R (version 4.3.1) to estimate variance–mean dependence and test for differential expression[68]. Genes with a Benjamini–Hochberg p-adjusted value ≤ 0.05 were defined differentially expressed, while those with a p-adjusted value ≤ 0.05 and an absolute $\log_2$ fold change ≥ 1 were identified as significantly differentially expressed genes (DEGs). A ranked list of the top DEGs is given in Supplementary Table S5. A principal component analysis was performed on transformed DESeq2 data (Supplementary Fig. S3). Sample-to-sample distance was calculated from the transformed count matrices and visualized as heatmap using the Pheatmap R package (version 1.0.12) (Supplementary Fig. S4). Both approaches indicated a clear separation among the A375-Ctrl and A375-hCYGB-derived data sets. In particular, PC1 accounted for 87% of the variance (Supplementary Fig. S3). Subsequently, we implemented fast gene set enrichment analysis (fGSEA) on the complete (normalized) count data[69] employing the hallmark gene sets[70]. For fGSEA (version 1.26.0) (https://bioconductor.org/packages/fgsea/) normalized count data was ranked and we included hallmark gene sets with a minimum of 25 and maximum of 500 genes. The Benjamini–Hochberg correction was used for p-value adjustment. Additionally, we conducted a gene ontology (GO) enrichment analysis on the DEGs employing GeneSCF (v1.1-p2) and the Gene Ontology Analysis (GOA) human GO list to define groups of genes based on their biological processes, molecular function, and cellular process, while

assessing their statistical significance[71]. The outcome was a compiled list of genes clustered organized according to their gene ontologies. To visually represent the findings of the differential expression analyses, we created volcano plots with the EnhancedVolcano R package (version 1.18.0; https://bioconductor.org/packages/EnhancedVolcano/). For the comparative DEG and hallmark analysis of hallmarks enriched in CYGB-dependent transcriptome between ectopic expression and shRNA-mediated knockdown of CYGB, we employed previously published data[5,9] available from GEO repository accession number GSE209775.

Comprehensive re-analysis of array datasets GSE29359 and GSE238207

Differential expression analysis of the publicly available microarray datasets GSE29359 and GSE238207 was performed in R using the limma package (version 3.56.2; https://bioconductor.org/packages/limma/)[72]. Genes with a p-adjusted value ≤ 0.05 were defined differentially expressed, while those with a p-adjusted value ≤ 0.05 and an absolute $\log_2$ fold change ≥ 1 were identified as significantly differentially expressed genes (DEGs). Using the results obtained from the differential expression analysis, we conducted fGSEA using the clusterProfiler package (version 4.8.3; https://bioconductor.org/packages/clusterProfiler/)[73]. The msigdbr package (version 7.5.1; https://bioconductor.org/packages/msigdb/) was used to extract both hallmark pathway (Figs. 6A and 7C) and gene ontology gene sets (Fig. 8B) from the Molecular Signatures Database (MSigDB). Volcano plots were created with the EnhancedVolcano R package (version 1.18.0).

Data availability

The data are contained with this article and supplementary files. RNA-sequencing raw data have been uploaded to the GEO repository (accession number GSE241816; weblink: https://www.ncbi.nlm.nih.gov/geo/query/acc.cgi?acc = GSE241816; temporary GSE data code: wpevcicqzzertop).

Received: 5 April 2024; Accepted: 1 August 2024
Published online: 06 August 2024

References

1. Burmester, T. & Hankeln, T. Function and evolution of vertebrate globins. *Acta Physiol. (Oxf.)* **211**, 501–514. https://doi.org/10.1111/apha.12312 (2014).
2. Keppner, A. *et al.* Lessons from the post-genomic era: Globin diversity beyond oxygen binding and transport. *Redox Biol.* **37**, 101687. https://doi.org/10.1016/j.redox.2020.101687 (2020).
3. Hankeln, T. *et al.* Neuroglobin and cytoglobin in search of their role in the vertebrate globin family. *J. Inorg. Biochem.* **99**, 110–119. https://doi.org/10.1016/j.jinorgbio.2004.11.009 (2005).
4. Fujita, Y. *et al.* Melanoma transition is frequently accompanied by a loss of cytoglobin expression in melanocytes: A novel expression site of cytoglobin. *PLoS One* **9**, e94772. https://doi.org/10.1371/journal.pone.0094772 (2014).
5. De Backer, J. *et al.* Cytoglobin silencing promotes melanoma malignancy but sensitizes for ferroptosis and pyroptosis therapy response. *Antioxidants (Basel)* **11**, 1548. https://doi.org/10.3390/antiox11081548 (2022).
6. De Backer, J. *et al.* The effect of reactive oxygen and nitrogen species on the structure of cytoglobin: A potential tumor suppressor. *Redox Biol.* **19**, 1–10. https://doi.org/10.1016/j.redox.2018.07.019 (2018).
7. Mathai, C., Jourd'heuil, F. L., Lopez-Soler, R. I. & Jourd'heuil, D. Emerging perspectives on cytoglobin, beyond NO dioxygenase and peroxidase. *Redox Biol.* **32**, 101468. https://doi.org/10.1016/j.redox.2020.101468 (2020).
8. Randi, E. B. *et al.* The antioxidative role of cytoglobin in podocytes: Implications for a role in chronic kidney disease. *Antioxid Redox Signal* **32**, 1155–1171. https://doi.org/10.1089/ars.2019.7868 (2020).
9. De Backer, J., Lin, A., Berghe, W. V., Bogaerts, A. & Hoogewijs, D. Cytoglobin inhibits non-thermal plasma-induced apoptosis in melanoma cells through regulation of the NRF2-mediated antioxidant response. *Redox Biol.* **55**, 102399. https://doi.org/10.1016/j.redox.2022.102399 (2022).
10. Gardner, A. M., Cook, M. R. & Gardner, P. R. Nitric-oxide dioxygenase function of human cytoglobin with cellular reductants and in rat hepatocytes. *J. Biol. Chem.* **285**, 23850–23857. https://doi.org/10.1074/jbc.M110.132340 (2010).
11. Halligan, K. E., Jourd'heuil, F. L. & Jourd'heuil, D. Cytoglobin is expressed in the vasculature and regulates cell respiration and proliferation via nitric oxide dioxygenation. *J. Biol. Chem.* **284**, 8539–8547. https://doi.org/10.1074/jbc.M808231200 (2009).
12. Liu, X. *et al.* Characterization of the function of cytoglobin as an oxygen-dependent regulator of nitric oxide concentration. *Biochemistry* **51**, 5072–5082. https://doi.org/10.1021/bi300291h (2012).
13. Liu, X. *et al.* Differences in oxygen-dependent nitric oxide metabolism by cytoglobin and myoglobin account for their differing functional roles. *FEBS J.* **280**, 3621–3631. https://doi.org/10.1111/febs.12352 (2013).
14. le Thuy, T. *et al.* Absence of cytoglobin promotes multiple organ abnormalities in aged mice. *Sci. Rep.* **6**, 24990. https://doi.org/10.1038/srep24990 (2016).
15. Liu, X. *et al.* Cytoglobin regulates blood pressure and vascular tone through nitric oxide metabolism in the vascular wall. *Nat. Commun.* **8**, 14807. https://doi.org/10.1038/ncomms14807 (2017).
16. Mimura, I. *et al.* Cytoglobin, a novel globin, plays an antifibrotic role in the kidney. *Am. J. Physiol. Renal Physiol.* **299**, F1120-1133. https://doi.org/10.1152/ajprenal.00145.2010ajprenal.00145.2010[pii] (2010).
17. Nishi, H. *et al.* Cytoglobin, a novel member of the globin family, protects kidney fibroblasts against oxidative stress under ischemic conditions. *Am. J. Pathol.* **178**, 128–139. https://doi.org/10.1016/j.ajpath.2010.11.011S0002-9440(10)00057-X[pii] (2011).
18. Schlosser, A. *et al.* The knockout of cytoglobin 1 in zebrafish (Danio rerio) alters lipid metabolism, iron homeostasis and oxidative stress response. *Biochim Biophys. Acta Mol. Cell Res.* **1870**, 119558. https://doi.org/10.1016/j.bbamcr.2023.119558 (2023).
19. Fordel, E., Geuens, E., Dewilde, S., De Coen, W. & Moens, L. Hypoxia/ischemia and the regulation of neuroglobin and cytoglobin expression. *IUBMB Life* **56**, 681–687. https://doi.org/10.1080/15216540500037406 (2004).
20. Fordel, E. *et al.* Cytoglobin expression is upregulated in all tissues upon hypoxia: an in vitro and in vivo study by quantitative real-time PCR. *Biochem. Biophys. Res. Commun.* **319**, 342–348. https://doi.org/10.1016/j.bbrc.2004.05.010 (2004).
21. Fordel, E. *et al.* Anoxia or oxygen and glucose deprivation in SH-SY5Y cells: A step closer to the unraveling of neuroglobin and cytoglobin functions. *Gene* **398**, 114–122. https://doi.org/10.1016/j.gene.2007.03.022 (2007).
22. Emara, M., Turner, A. R. & Allalunis-Turner, J. Hypoxic regulation of cytoglobin and neuroglobin expression in human normal and tumor tissues. *Cancer Cell Int.* **10**, 33. https://doi.org/10.1186/1475-2867-10-33 (2010).
23. Guo, X., Philipsen, S. & Tan-Un, K. C. Study of the hypoxia-dependent regulation of human CYGB gene. *Biochem Biophys. Res. Commun.* **364**, 145–150. https://doi.org/10.1016/j.bbrc.2007.09.108 (2007).

24. Langan, J. E. *et al.* Novel microsatellite markers and single nucleotide polymorphisms refine the tylosis with oesophageal cancer (TOC) minimal region on 17q25 to 42.5 kb. *Hum. Genet.* **114**, 534–540. https://doi.org/10.1007/s00439-004-1100-3 (2004).
25. McRonald, F. E. *et al.* Down-regulation of the cytoglobin gene, located on 17q25, in tylosis with oesophageal cancer (TOC): evidence for trans-allele repression. *Hum. Mol. Genet.* **15**, 1271–1277. https://doi.org/10.1093/hmg/ddl042 (2006).
26. Shivapurkar, N. *et al.* Cytoglobin, the newest member of the globin family, functions as a tumor suppressor gene. *Cancer Res.* **68**, 7448–7456. https://doi.org/10.1158/0008-5472.CAN-08-0565 (2008).
27. Shaw, R. J. *et al.* Cytoglobin is upregulated by tumour hypoxia and silenced by promoter hypermethylation in head and neck cancer. *Br. J. Cancer* **101**, 139–144. https://doi.org/10.1038/sj.bjc.6605121 (2009).
28. Xu, H. W. *et al.* The expression of cytoglobin as a prognostic factor in gliomas: a retrospective analysis of 88 patients. *BMC Cancer* **13**, 247 (2013).
29. Oleksiewicz, U. *et al.* Cytoglobin has bimodal: Tumour suppressor and oncogene functions in lung cancer cell lines. *Hum. Mol. Genet.* **22**, 3207–3217. https://doi.org/10.1093/hmg/ddt174 (2013).
30. John, R. *et al.* Cell cycle-dependent regulation of cytoglobin by Skp2. *FEBS Lett.* **591**, 3507–3522. https://doi.org/10.1002/1873-3468.12864 (2017).
31. le Thuy, T. *et al.* Cytoglobin deficiency promotes liver cancer development from hepatosteatosis through activation of the oxidative stress pathway. *Am. J. Pathol.* **185**, 1045–1060. https://doi.org/10.1016/j.ajpath.2014.12.017 (2015).
32. Yassin, M. *et al.* Cytoglobin affects tumorigenesis and the expression of ulcerative colitis-associated genes under chemically induced colitis in mice. *Sci. Rep.* **8**, 6905 (2018).
33. le Thuy, T. *et al.* Promotion of liver and lung tumorigenesis in DEN-treated cytoglobin-deficient mice. *Am. J. Pathol.* **179**, 1050–1060. https://doi.org/10.1016/j.ajpath.2011.05.006 (2011).
34. Hoang, D. V. *et al.* Cytoglobin attenuates pancreatic cancer growth via scavenging reactive oxygen species. *Oncogenesis* **11**, 23. https://doi.org/10.1038/s41389-022-00389-4 (2022).
35. Chakraborty, S., John, R. & Nag, A. Cytoglobin in tumor hypoxia: novel insights into cancer suppression. *Tumour Biol.* **35**, 6207–6219. https://doi.org/10.1007/s13277-014-1992-z (2014).
36. Bholah, T. C., Neergheen-Bhujun, V. S., Hodges, N. J., Dyall, S. D. & Bahorun, T. Cytoglobin as a biomarker in cancer: Potential perspective for diagnosis and management. *Biomed. Res. Int.* **2015**, 824514 (2015).
37. Reeder, B. J. Insights into the function of cytoglobin. *Biochem. Soc. Trans.* **51**, 1907–1919. https://doi.org/10.1042/BST20230081 (2023).
38. Zou, Z., Tao, T., Li, H. & Zhu, X. mTOR signaling pathway and mTOR inhibitors in cancer: progress and challenges. *Cell Biosci.* **10**, 31. https://doi.org/10.1186/s13578-020-00396-1 (2020).
39. Mossmann, D., Park, S. & Hall, M. N. mTOR signalling and cellular metabolism are mutual determinants in cancer. *Nat. Rev. Cancer* **18**, 744–757. https://doi.org/10.1038/s41568-018-0074-8 (2018).
40. Dowling, R. J., Topisirovic, I., Fonseca, B. D. & Sonenberg, N. Dissecting the role of mTOR: lessons from mTOR inhibitors. *Biochim Biophys. Acta* **433–439**, 2010. https://doi.org/10.1016/j.bbapap.2009.12.001 (1804).
41. Stengel, S. *et al.* Suppression of MYC by PI3K/AKT/mTOR pathway inhibition in combination with all-trans retinoic acid treatment for therapeutic gain in acute myeloid leukaemia. *Br. J. Haematol.* **198**, 338–348. https://doi.org/10.1111/bjh.18187 (2022).
42. Gabay, M., Li, Y. & Felsher, D. W. MYC activation is a hallmark of cancer initiation and maintenance. *Cold Spring Harb Perspect Med* **4** (2014).
43. Drosten, M. & Barbacid, M. Targeting the MAPK pathway in KRAS-driven tumors. *Cancer Cell* **37**, 543–550. https://doi.org/10.1016/j.ccell.2020.03.013 (2020).
44. Ueda, Y. & Richmond, A. NF-kappaB activation in melanoma. *Pigment Cell Res.* **19**, 112–124 (2006).
45. Rubin, L. L. & de Sauvage, F. J. Targeting the Hedgehog pathway in cancer. *Nat. Rev. Drug Discov.* **5**, 1026–1033. https://doi.org/10.1038/nrd2086 (2006).
46. Price, M. A. *et al.* CSPG4, a potential therapeutic target, facilitates malignant progression of melanoma. *Pigment Cell Melanoma Res.* **24**, 1148–1157 (2011).
47. Yang, J. *et al.* Melanoma chondroitin sulfate proteoglycan enhances FAK and ERK activation by distinct mechanisms. *J. Cell Biol.* **165**, 881–891 (2004).
48. Yang, J. *et al.* Melanoma proteoglycan modifies gene expression to stimulate tumor cell motility, growth, and epithelial-to-mesenchymal transition. *Cancer Res.* **69**, 7538–7547 (2009).
49. Uranowska, K. *et al.* Expression of chondroitin sulfate proteoglycan 4 (CSPG4) in melanoma cells is downregulated upon inhibition of BRAF. *Oncol. Rep.* **45**, 14. https://doi.org/10.3892/or.2021.7965 (2021).
50. Gomes, B. R. B. *et al.* Cytoglobin attenuates neuroinflammation in lipopolysaccharide-activated primary preoptic area cells via NF-κB pathway inhibition. *Front. Mol. Neurosci.* https://doi.org/10.3389/fnmol.2019.00307 (2019).
51. Ou, L. *et al.* Recombinant human cytoglobin prevents atherosclerosis by regulating lipid metabolism and oxidative stress. *J. Cardiovasc. Pharmacol. Ther.* **23**, 162–173. https://doi.org/10.1177/1074248417724870 (2018).
52. Trandafir, F. *et al.* Neuroglobin and cytoglobin as potential enzyme or substrate. *Gene* **398**, 103–113. https://doi.org/10.1016/j.gene.2007.02.038 (2007).
53. Zweier, J. L. *et al.* Cytoglobin has potent superoxide dismutase function. *Proc. Natl. Acad. Sci. USA* **118** (2021).
54. Mathai, C. *et al.* Regulation of DNA damage and transcriptional output in the vasculature through a cytoglobin-HMGB2 axis. *Redox Biol.* **65**, 102838. https://doi.org/10.1016/j.redox.2023.102838 (2023).
55. Hartman, M. L. & Czyz, M. MITF in melanoma: mechanisms behind its expression and activity. *Cell Mol. Life Sci.* **72**, 1249–1260 (2015).
56. Kawakami, A. & Fisher, D. E. The master role of microphthalmia-associated transcription factor in melanocyte and melanoma biology. *Lab. Investig.* **97**, 649–656. https://doi.org/10.1038/labinvest.2017.9 (2017).
57. Oliveira, C. S. *et al.* Macrophage migration inhibitory factor engages PI3K/Akt signalling and is a prognostic factor in metastatic melanoma. *BMC Cancer* **14**, 630 (2014).
58. Tanese, K. *et al.* Cell surface CD74-MIF interactions drive melanoma survival in response to interferon-γ. *J. Invest Dermatol.* **135**, 2775–2784 (2015).
59. Fukuda, Y. *et al.* Interplay between soluble CD74 and macrophage-migration inhibitory factor drives tumor growth and influences patient survival in melanoma. *Cell Death Dis.* **13**, 117. https://doi.org/10.1038/s41419-022-04552-y (2022).
60. Passarelli, A., Mannavola, F., Stucci, L. S., Tucci, M. & Silvestris, F. Immune system and melanoma biology: A balance between immunosurveillance and immune escape. *Oncotarget* **8**, 106132–106142 (2017).
61. Haanen, J. B. A. G. Immunotherapy of melanoma. *Eur. J. Cancer Suppl.* **11**, 97–105. https://doi.org/10.1016/j.ejcsup.2013.07.013 (2013).
62. Koay, T. W. *et al.* Androglobin gene expression patterns and FOXJ1-dependent regulation indicate its functional association with ciliogenesis. *J. Biol. Chem.* **296**, 100291. https://doi.org/10.1016/j.jbc.2021.100291 (2021).
63. Storti, F. *et al.* A novel distal upstream hypoxia response element regulating oxygen-dependent erythropoietin gene expression. *Haematologica* **99**, e45-48. https://doi.org/10.3324/haematol.2013.102707 (2014).
64. De Backer, J., Maric, D., Bosman, M., Dewilde, S. & Hoogewijs, D. A reliable set of reference genes to normalize oxygen-dependent cytoglobin gene expression levels in melanoma. *Sci. Rep.* **11**, 10879 (2021).

65. Schörg, A. *et al.* Destruction of a distal hypoxia response element abolishes trans-activation of the *PAG1* gene mediated by HIF-independent chromatin looping. *Nucleic Acids Res.* **43**, 5810–5823. https://doi.org/10.1093/nar/gkv506 (2015).
66. Keppner, A. *et al.* Androglobin, a chimeric mammalian globin, is required for male fertility. *eLife* **11**, e72374. https://doi.org/10.7554/eLife.72374 (2022).
67. Orlando, I. M. C. *et al.* Distal and proximal hypoxia response elements cooperate to regulate organ-specific erythropoietin gene expression. *Haematologica* **105**, 2774–2784. https://doi.org/10.3324/haematol.2019.236406 (2020).
68. Love, M. I., Huber, W. & Anders, S. Moderated estimation of fold change and dispersion for RNA-seq data with DESeq2. *Genome Biol* **15**, 550 (2014).
69. Korotkevich, G. *et al.* (bioRxiv, 2016).
70. Liberzon, A. *et al.* The molecular signatures database (MSigDB) hallmark gene set collection. *Cell Syst.* **1**, 417–425 (2015).
71. Huntley, R. P. *et al.* The GOA database: Gene ontology annotation updates for 2015. *Nucleic Acids Res.* **43**, D1057-1063 (2015).
72. Ritchie, M. E. *et al.* limma powers differential expression analyses for RNA-sequencing and microarray studies. *Nucleic Acids Res.* **43**, e47 (2015).
73. Wu, T. *et al.* clusterProfiler 4.0: A universal enrichment tool for interpreting omics data. *Innovation (Camb)* **2**, 100141 (2021).
74. Herwig, A. *et al.* Ectopic MYBL2-mediated regulation of androglobin gene expression. *Cells* **13**, 826. https://doi.org/10.3390/cells13100826 (2024).

Acknowledgements

J.D.B. acknowledges a visiting fellowship from the University of Fribourg. D.H. acknowledges support by the Swiss National Science Foundation (Grant 310030_207460).

Author contributions

J.D.B. and D.H. conceptualization; J.D.B. methodology; J.D.B. investigation; J.D.B. visualization; J.D.B. and D.H. writing—original draft preparation; D.H. funding acquisition. Both authors reviewed the manuscript.

Competing interests

The authors declare no competing interests.

Additional information

Supplementary Information The online version contains supplementary material available at https://doi.org/10.1038/s41598-024-69224-7.

Correspondence and requests for materials should be addressed to D.H.